Journal of Hydroscience and Hydraulic Engineering
Vol. 20, No.1 May, 2002, 77-93

INCIPIENT OSCILLATIONS OF A SHEET OF FALLING WATER AND THE INSTABILITY MECHANISMS

By

H. Kyotoh

Institute of Engineering Mechanics and Systems, University of Tsukuba, Ibaraki, Japan

R. Nakamura

Third Plan Design Industrial Co., Ltd., Gifu, Japan

and

P. J. Baruah

Doctoral Program in Engineering, University of Tsukuba, Ibaraki, Japan

SYNOPSIS

Water surface displacements at various heights of the sheet were measured to find and to investigate the region of initiation of the sheet oscillations, i.e., the incipient oscillations. The power spectra show that a sinuous oscillation appears upstream and a super-harmonic transition occurs downstream. To calculate the impedance of the sheet, periodic forced-vibrations were applied at the weir crest. The frequency response of the sheet varied with position along the sheet and, therefore, with the thickness of the sheet. Also, the geometry of the air space behind the sheet was confined with a back wall of adjustable length. By varying the length of the plate, we observed pressure fluctuations propagating upstream. From these results, an integro-differential equation was developed to model the motion of the sheet. The numerical solution of this equation reproduces the tendency of the amplitude of oscillation of the sheet to grow exponentially along the sheet and the resonance between the sheet and the confined air behind the sheet. Moreover, incipient oscillations of the sheet were characterized through a linear stability analysis of the Navier –Stokes equation.

1. INTRODUCTION

Oscillations of a sheet of falling water have been studied in relation to the nappe oscillations of weirs and dams (e.g., Shwartz (1), Binnie (2) and Honma and Ogiwara (3)). Recently, civil and environmental engineers have been concerned with the noise produced from these oscillations, and the efficiency of momentum and heat exchanges between air and water. The prediction and control of the sheet breakup height are also important for the design of fountains (Casperson (4)). Also, stabilizing a plane liquid sheet is essential for film coatings (e.g., Weinstein et al. (5) and Luca (6)), while disintegration of liquid is necessary for the mixing of fuel and gas (e.g., Lasheras and Hopfinger (7)).

Taylor ((8) and (9)) studied the dynamics of thin sheets of fluid, and discussed the free-edge shape of the liquid sheets and their disintegration based on the surface wave dynamics. Research in this area has been extended to the investigation of liquid atomization problems (e.g., Mansour and Chigier (10)), where shear stresses from air and surface tension govern the breakup regime (Lasheras and Hopfinger (7)). On the other hand, a falling liquid sheet is gradually accelerated by the gravitational force, and then both shear stresses between air and water and pressure fluctuations propagating through air influence the sheet motion (Binnie (2) and Kyotoh and Kase (11)), thus resulting in large

amplitude oscillations. In these studies, the sheet is abruptly amplified at around two meters downstream from the weir crest and the wavelength of sheet oscillations is about 60 cm (see also Aizawa and Shinohara(12)). Since the flow is non-uniform and convective, i.e., the thickness and the falling velocity change roughly from 2 cm to 1 mm and from 3 cm/s to 6 m/s respectively, it might be difficult to decide the origin of the instability leading to such a large amplitude sheet oscillation. Therefore, in the present study the displacement of the water sheet is measured starting from the point of fall down to the breakup point to observe the spatial evolution of the oscillation.

The mechanism of liquid sheet instability and breakup has been studied theoretically by numerous authors. Hagerty and Shea (13) found that only two types of waves are possible on a flat liquid sheet, i.e., sinuous and dilational modes. Lin (14) showed that a viscous liquid curtain becomes unstable when the Weber number of the curtain flow exceeds 1/2. Luca and Costa (15) studied the instability of a spatially developing liquid sheet by using a multiple-scale perturbation analysis. They showed that the sinuous mode is locally absolutely unstable below a critical Weber number, and that it is locally convectively unstable if the Weber number exceeds this critical value. Weinstein et al. (5) derived approximate equations that govern the time-dependent response of a two-dimensional liquid curtain falling under the influence of gravity and subjected to ambient pressure disturbances. As aforementioned in regard to the falling-water sheet, pressure fluctuations due to sheet movements and shear stresses from ambient air should be considered in the modeling.

The present investigation was undertaken to address some of the questions raised above. In section 2, experimental results obtained from "free falls", "free falls with vibrations", and "free falls with a back wall"(with or without vibrations), are presented. In section 3, a model which describes the motion of the two-dimensional sheet is developed, and shear waves which were observed in this study are characterized by a linear stability analysis of the Navier –Stokes equations.

2. EXPERIMENT

2.1 EXPERIMENTAL SETUP

The experimental apparatus is illustrated in Fig. 1. The free fall of the water from the weir is confined between two side walls, one being transparent and another a black-painted ply-board. The weir has a width of 40 cm and a height of 40 cm. The water falling from the weir to a bottom tank is circulated with a centrifugal pump.

The following equipment was used in the experiments for collection of data.

(a) A high-speed video camera is used to capture images of the falling stream. The camera records 186 frames per second, which has a maximum recording capacity of 256 frames per second in normal mode.

(b) Transverse motion of the water sheet is monitored with a laser-beam displacement sensor. The sampling time and the amount of data to be recorded can be set independently. Some whitening material is mixed in the water for proper visualization and acquisition of data.

(c) A system to apply a forced vibration is installed at the weir tank near the spillway.

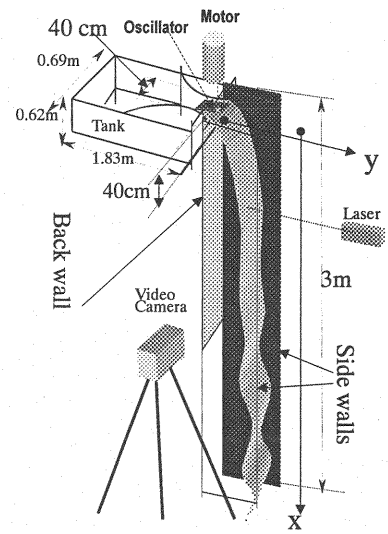

Fig. 1 Experimental setup

2.2 EXPERIMENTAL RESULTS

Experiments were performed for mainly three cases, "free falls without forced vibrations", "free falls with periodic forced vibrations" and "free falls with a back wall". For each set of experiments, the displacement of the water sheet was measured with the laser displacement sensor starting from the

point of the fall in intervals of 10 cm down to 250 cm from the top. The footage taken by the high-speed video camera was used to find the wave period and celerity, to estimate the breakup point, and also to study other structural features of the phenomena.

2.2.1 FREE FALLS EXPERIMENT

Figure 2 shows the power spectra of the sheet displacement at 0 cm, 120 cm and 220 cm from the weir crest for two discharges, Q = 0.130 m^3/min and 0.189 m^3/min. The spectra are plotted from 3 Hz to 50 Hz. Incipient oscillations, i.e., the oscillations which appear first along the sheet, are observed at x = 120 cm, and these frequencies are 10 Hz in Fig. 2(a) and 15 Hz in Fig. 2(b). Our aim was to find the origin of the unstable mode related to the breakup frequency around 30 Hz, which was calculated from the displacements of the wave crests and troughs, as shown in Fig. 3. The sub-harmonic frequencies of 10 Hz and 15 Hz suggest that a super-harmonic bifurcation might occur somewhere between x = 120 cm and the breakup region. In a forced-vibration experiment discussed in 2.2.2, the upper part of the sheet does not respond strongly to these high frequency oscillations. Therefore, it was concluded that the instability leading to the sheet breakup is mainly caused by events occurring near the breakup region.

The length and time scales of the sheet breakup are measured from the video camera images as shown in Fig. 3. The frequency was found to be around 30 Hz and the corresponding wavelength is roughly 60 cm. Here, the wave celerity is taken to be approximately equal to the flow velocity. The figure shows that the wave celerity increases when the discharge decreases.

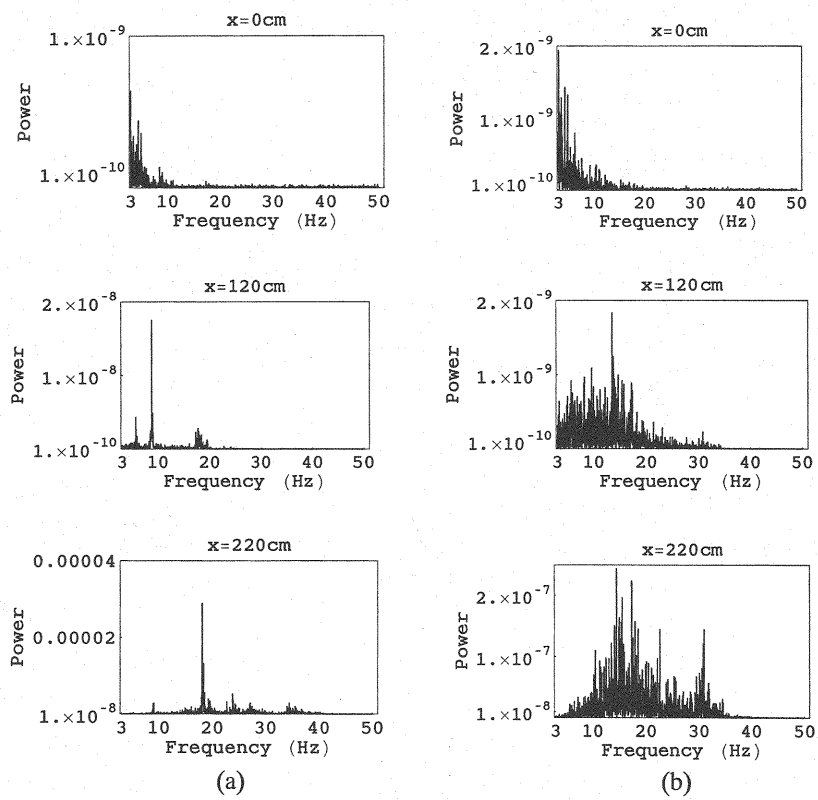

Fig. 2 Spatial dependence of the spectra of sheet oscillations
(a) h_e = 2.12cm, Q = 0.130 m^3/min, (b) h_e = 3.47 cm, Q = 0.189 m^3/min
(h_e is the water depth above the weir.)

2.2.2 FREE FALLS EXPERIMENT WITH VIBRATIONS

Forced vibrations of roughly 1 mm in amplitude were applied at the water surface near the weir crest. Figure 4 shows the logarithm of the sheet amplitude normalized by that at x=0 cm for various forced frequencies. The figure indicates that the higher frequencies such as 15 Hz and 20 Hz have greater influence on the downstream portion of sheet, i.e. the thinner section of the sheet. The growth rates of all the imposed frequencies are exponential. The imposed frequency of 15Hz has the highest growth rate near the breakup point.

2.2.3 FREE FALLS EXPERIMENT WITH A BACK WALL.

In order to reveal the effects of the air confined behind the water sheet, the length of the back wall was changed from 40 cm to 90 cm and then to180 cm. Note that the weir height is 40 cm (see Fig. 1). Figure 5 shows the root mean square values of the sheet's amplitude of oscillation. As the wall length increases, the amplitude of oscillation increases, and an amplitude modulation appears especially well-pronounced for the 180 cm wall. This modulation is caused by a prominent water advancing upstream under the influence of pressure fluctuations of the confined air.

2.2.4 OTHER EXPERIMENTAL RESULTS

Figure 6 shows a typical side view and the front view of the falling water sheet under forced vibration. The growth of a wave is clearly seen in the side view. The front view shows how the water sheet starts to detach from the side-walls upstream of the breakup region, thus amplifying the sheet amplitude. Further downstream, the transverse and longitudinal structures (vortices and waves) become more prominent. Ligaments originating from these longitudinal and transverse structures break up into water drops after the water sheet is disrupted.

3. THEORETICAL DISCUSSION

The prediction of frequency of the waves leading to sheet breakup becomes a difficult task, mainly because the flow is of non-uniform and convective nature. Thus, the length scales change

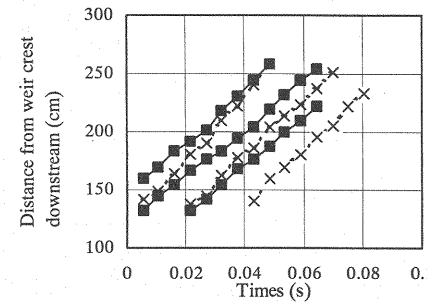

Fig. 3 Displacement of wave crests and troughs (Solid line; Q = 0.189 m^3/min, Dashed line; Q = 0.155 m^3/min)

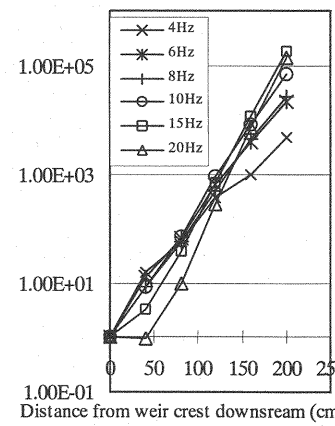

Fig. 4 Amplification rate of the power in forced vibration experiments (Q = 0.139 m^3/min)

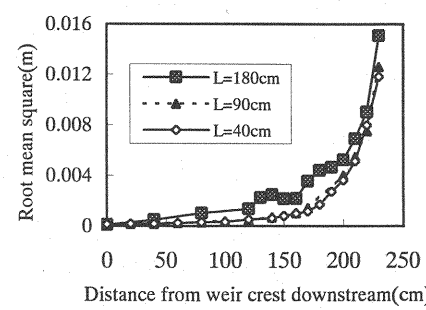

Fig. 5 Amplitude of sheet oscillations with a back wall (Q = 0.155 m^3/min and L is the length of back wall)

downstream, and the fluctuations generated upstream propagate downstream, and vice versa. The physical factors affecting the motion of a falling water sheet are summarized as follows:
(A) The propagation of pressure fluctuations under the influence of confined air.
(B) The shear wave instability of air flow induced by the falling water.
(C) Surface tension effects on the water sheet.
Factor (A) is predominant if air is confined between the water sheet and the side and back walls. Factor (B) is significant if the height of the fall is large. Factor (C) is predominant at smaller length scales of the fluid. Though all of the above factors are concerned with sheet oscillations, only the Kelvin-Helmholtz instability, which is related to factor (A), and the shear wave instability between air and water will be the focus of this section. In addition, to facilitate the analyses in the present section, we will study "a sheet of vertically falling water".

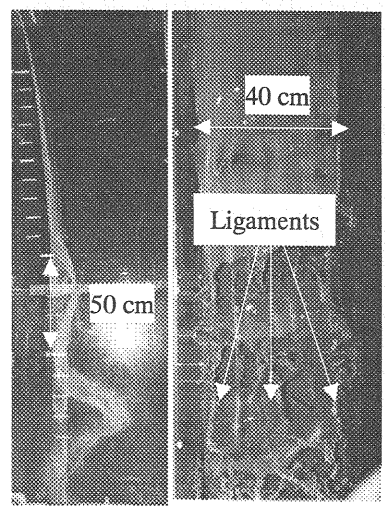

Fig. 6 Typical side view and front view of a free fall under forced vibration
(Q = 0.139 m^3/min, the frequency is 15 Hz)

3.1 THE KELVIN-HELMHOLTZ INSTABILITY

When the air in the front and back of a falling water sheet is enclosed by vertical walls and upper and lower boundaries, the effect of a local sheet displacement influences the other parts of the sheet. Here, the flow is assumed to be irrotational because we want to consider only the global motion of the sheet, and thus shear waves between the water and air are ignored. In order to apply the model derived in the present study for various boundary geometries, the equations for the water sheet and air are derived separately.

3.1.1 GOVERNING EQUATIONS

The governing equations for water are the Laplace and pressure equations given by

$$\Delta\phi_w = 0$$

$$\frac{\partial\phi_w}{\partial t} + \frac{1}{2}\left[\left(\frac{\partial\phi_w}{\partial x}\right)^2 + \left(\frac{\partial\phi_w}{\partial y}\right)^2\right] - gx + \frac{P_w}{\rho_w} = 0 \qquad (1)$$

where, Δ denotes the two-dimensional Laplace operator with variables x and y, and, ϕ_w and P_w are the velocity potential and pressure, respectively. The subscript "w" denotes the water sheet; ρ_w = the water density; g = the gravity acceleration; t = the time and x and y = the spatial coordinates, where x is taken positive vertically downward. The boundary conditions for the water at the interfaces between the water and the air are pressure and kinematic conditions given by

$$P_w + S\kappa_\alpha - P_{S\alpha} = 0 \;; \quad \frac{\partial\eta_\alpha}{\partial t} + \frac{\partial\phi_w}{\partial x}\frac{\partial\eta_\alpha}{\partial x} - \frac{\partial\phi_w}{\partial y} = 0 \qquad (2)$$
$$at \quad y = \eta_\alpha; \quad \alpha = r, \ell$$

where the suffix "α" can be "r" or "ℓ", which denote the right- and left-hand sides of the water sheet, respectively. $P_{S\alpha}$ is the air pressure at the interface; S = the surface tension coefficient; κ_α = the interface curvature; and η_α = the displacement of the water sheet.

In the present study, we consider sheet motions in which the vertical scale is much greater than the horizontal, thus resulting in the scaling

$$O(\partial / \partial x) / O(\partial / \partial y) = \varepsilon << 1 \tag{3}$$

Moreover, it is assumed that the acceleration of the liquid is of the order of gravity (Weinstein et al. (5)). Under these assumptions, the series expansions of the unknowns with respect to $\delta \equiv \varepsilon^2$ are

$$\begin{aligned} \eta_\alpha &= \eta_{\alpha 0}(\varepsilon x, t) + \delta \eta_{\alpha 1}(\varepsilon x, t) + \ldots \\ \phi_w &= \phi_{w0}(\varepsilon x, y, t) + \delta \phi_{w1}(\varepsilon x, y, t) + \ldots \\ P_{S\alpha} &= P_{S\alpha 0}(\varepsilon x, t) + \delta P_{S\alpha 1}(\varepsilon x, t) + \ldots \\ \delta &\equiv \varepsilon^2 \end{aligned} \tag{4}$$

Note that these unknowns depend on the slow variable εx and that the displacement $\eta_{\alpha 0}$ is of order unity, which means the amplitude of the oscillations are finite. The lowest order equations obtained from the series equations are

$$\frac{\partial Y_s}{\partial t} + \frac{\partial}{\partial x}(U_w Y_s) = 0 \tag{5a}$$

$$\rho_w \left(\frac{\partial U_w}{\partial t} + U_w \frac{\partial U_w}{\partial x} \right) = (\rho_w - \rho_a) g \tag{5b}$$

$$\frac{\partial}{\partial t}(2\rho_w Y_s V_w) + \frac{\partial}{\partial x}(2\rho_w Y_s U_w V_w) - 2S \frac{\partial^2 Y_m}{\partial x^2} = P_{S\ell 1} - P_{Sr1} \tag{5c}$$

$$V_w \equiv \frac{\partial Y_m}{\partial t} + \frac{\partial Y_m}{\partial x} U_w$$

where

$$U_w = \frac{\partial \phi_{w0}}{\partial x} \quad ; \quad Y_s = \frac{1}{2}(\eta_{r0} - \eta_{\ell 0}) \quad ; \quad Y_m = \frac{1}{2}(\eta_{r0} + \eta_{\ell 0}) \tag{5d}$$

Equation 5a reflects the conservation of volume, Eqs. 5b and 5c are the momentum conservation laws for the vertical and horizontal directions, respectively. These equations constitute a chain system; i.e., U_w is determined from Eq. 5b alone, Y_s is obtained from Eq. 5a without solving Eq. 5c, and then Y_m can be solved after these calculations. Note that the pressure $P_{S\alpha}$ becomes a function of the interface displacement η_α.

To determine the pressure, the Laplace equation for the potential function for the air flow should be solved under the kinematic boundary conditions, i.e., the continuity of the normal velocity at the interface and the non-penetrability of the surrounding fixed boundaries. In the first stage of this study, we considered the motion of a water sheet in which the displacements from the vertical plane are small, and the region of confined air is rectangular (see Fig. 7). Then, the potential function for the air flow is determined from

$$\Delta\phi_{\alpha 1} = 0$$

$$\left.\frac{\partial\phi_{\alpha 1}}{\partial y}\right|_{y=0} = \frac{\partial\eta_{\alpha 0}}{\partial t} \;;\; \left.\frac{\partial\phi_{\alpha 1}}{\partial y}\right|_{y=L_\alpha} = 0$$

$$\left.\frac{\partial\phi_{\alpha 1}}{\partial x}\right|_{x=0} = 0 \;;\; \left.\frac{\partial\phi_{\alpha 1}}{\partial x}\right|_{x=h} = 0 \qquad (6)$$

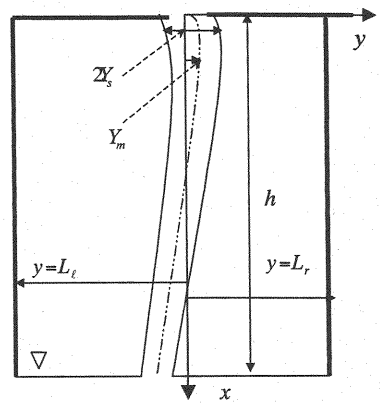

Fig. 7 Schematic picture of the side view and the geometry of the vertical falling water

where L_α is the position of the wall ($L_r > 0$, $L_\ell < 0$ in Fig. 7), and h is the height of the walls (see Fig. 7). Note that the sheet thickness relative to the horizontal distance from the back wall to the water surface has been ignored since $Y_s << |L_\alpha|$. After obtaining the potential function by applying the method of separation of variables, the value of the potential function $\phi_{S\alpha 1}$ at the interface is represented by the integral

$$\phi_{S\alpha 1}(x,t) = 2\int_0^h G_\alpha(x/h,\bar{x}/h)\frac{\partial\eta_{\alpha 0}}{\partial t}(\bar{x},t)\,d\bar{x}$$

$$G_\alpha(x/h,\bar{x}/h) = -\frac{1}{\pi}\sum_{n=1}^{\infty}\frac{\cos\frac{n\pi x}{h}\cos\frac{n\pi\bar{x}}{h}}{n\tanh\left(\frac{n\pi L_\alpha}{h}\right)}, \quad \alpha = r,\ell \qquad (7)$$

which is applicable for any h/L_α. Here, the constant pressure difference between each side of the sheet has been ignored. The pressure $P_{S\alpha 1}$ at the interface is calculated from the pressure equation by differentiating the potential shown in Eq. 7 with respect to t, which leads to

$$P_{S\alpha 1}(x,t) = -2\rho_a\int_0^h G_\alpha(x/h,\bar{x}/h)\frac{\partial^2\eta_{\alpha 0}}{\partial t^2}(\bar{x},t)\,d\bar{x}, \quad \alpha = r,\ell \qquad (8)$$

Finally, Eqs. 5a, 5b, 5c and 8 constitute the closed system of equations for small amplitude motions of the water sheet.

3.1.2 ANALYSIS OF THE SHEET OSCILLATIONS

Equations 5a and 5b can be solved analytically by using the characteristic method, which leads to

$$x = \frac{g_0}{2}(t-\tau)^2 + u_{e0}(\tau)(t-\tau)$$

$$U_w = g_0(t-\tau) + u_{e0}(\tau) \tag{9}$$

$$Y_s = \frac{u_{e0}(\tau)y_{e0}(\tau)}{g_0(t-\tau)+u_{e0}(\tau)}$$

where $g_0 = (1-\rho_a/\rho_w)g$, $u_{e0}(\tau)$ and $y_{e0}(\tau)$ are respectively the values of U_w and Y_s at $x=0$ and $t=\tau$, and τ is the intermediate parameter ranging in value from 0 to t. Since the sinuous mode (Hagerty and Shea (13)) of the sheet seems to be realized in the present experiment (see Fig. 6), $u_{e0}(\tau)$ and $y_{e0}(\tau)$ are taken to be independent of τ. Then, U_w and Y_s are represented by a function of x if τ is eliminated from Eq. 9. Substituting these values into Eq. 5c, the governing equation of Y_m with respect to the following non-dimensional variables (Eq. 10)

$$x_n = \frac{x}{h};\ t_n = t\sqrt{\frac{g_0}{h}};\ q_n = \frac{2u_{e0}y_{e0}}{h\sqrt{g_0 h}};\ u_{e0n} = \frac{u_{e0}}{\sqrt{2g_0 h}};\ W_b = \frac{S}{2\rho_w u_{e0}y_{e0}\sqrt{g_0 h}} \tag{10}$$

is written as

$$\begin{aligned} &2\sqrt{x_n+u_{e0n}{}^2}\left(\sqrt{x_n+u_{e0n}{}^2}-\sqrt{2}W_b\right)\frac{\partial^2 Y_m}{\partial x_n{}^2}+2\sqrt{2}\sqrt{x_n+u_{e0n}{}^2}\,\frac{\partial^2 Y_m}{\partial t_n \partial x_n}+\frac{\partial^2 Y_m}{\partial t_n{}^2}+\frac{\partial Y_m}{\partial x_n} \\ &=2\sqrt{2}\sqrt{x_n+u_{e0n}{}^2}\,\frac{\gamma}{q_n}\int_0^1\{G_r(x_n,x_{nI})-G_\ell(x_n,x_{nI})\}\frac{\partial^2 Y_m}{\partial t_n{}^2}(x_{nI},t_n)dx_{nI} \end{aligned} \tag{11}$$

where, q_n is the non-dimensional discharge for unit width and γ is the density ratio defined by ρ_a/ρ_w. The effect of air on the water sheet is represented by γ/q_n, which is of order unity for a small discharge or for the large height h even if the density ratio is low. Though Eq. 11 is linear, it has several interesting physical features: the flow is spatially non-uniform, local disturbances downstream propagate upstream because of the integral term of Eq. 11, and the principal part of Eq. 11 changes its type from hyperbolic to parabolic at the point where the coefficient of the second order derivative of Y_m is identical to zero.

We will focus on temporally harmonic motions, so the solution of Eq. 11 is

$$Y_m(x_n,t_n) = A_{Ym}(x_n)e^{i\Omega t_n} \tag{12}$$

where, Ω is a non-dimensional angular frequency. Substitution of Eq. 12 into Eq. 11 leads to

$$\begin{aligned} &2\sqrt{x_n+u_{e0n}{}^2}\left(\sqrt{x_n+u_{e0n}{}^2}-\sqrt{2}W_b\right)\frac{d^2 A_{Ym}}{dx_n{}^2}+\left(1+2\sqrt{2}i\Omega\sqrt{x_n+u_{e0n}{}^2}\right)\frac{dA_{Ym}}{dx_n}-\Omega^2 A_{Ym} \\ &=-2\sqrt{2}\sqrt{x_n+u_{e0n}{}^2}\,\frac{\gamma}{q_n}\Omega^2\int_0^1\{G_r(x_n,x_{nI})-G_\ell(x_n,x_{nI})\}A_{Ym}(x_{nI})dx_{nI} \end{aligned} \tag{13}$$

The boundary conditions for Eq. 13 should be defined depending on the type of partial differential equation (abbr. PDE) so that the system becomes well-posed. Since the type of PDE is categorized by the position of the singular point, $x_n = x_{nS}$; satisfying

$$\sqrt{x_{nS}+u_{e0n}{}^2}-\sqrt{2}W_b=0 \tag{14}$$

where, the second order derivative in Eq. 13 disappears if it is not infinite at this point, the boundary values for Eq. 13 should be imposed on

(i) $A_{Ym}(0)$ and $\dfrac{dA_{Ym}}{dx_n}(0)$, for $x_{nS}<0$,
(ii) $A_{Ym}(0)$ and $A_{Ym}(1)$, for $x_{nS}>1$,
(iii) $A_{Ym}(x_{nS})$, for $0<x_{nS}<1$.

In the case (iii), the value of $A_{Ym}(x_{nS})$ forces a dependence of $A_{Ym}(0)$ on $dA_{Ym}/dx_n(0)$ so that a smooth solution exists. A similar situation occurs for steady flow when a constant pressure difference is applied to the sheet (Finnicum et al. (16)).

Since $W_b << u_{e0n}/\sqrt{2}$ in our experiment, it is reasonable to put $W_b \approx 0$. Consistent with the discussion above, the two boundary conditions

$$A_{Ym}(0)=0 \quad \text{and} \quad \frac{dA_{Ym}}{dx_n}(0)=1 \tag{15}$$

are imposed in the present study. To facilitate the numerical calculations, Eq. 13 is transformed into an integral equation satisfying these boundary conditions as follows:

$$A_{Ym}(x_n)-\Gamma\Omega^2\int_0^1 A_{Ym}(x_{nJ})G_f(x_n,x_{nJ})dx_{nJ}=F(x_n),\quad \Gamma\equiv 2\sqrt{2}\gamma/q_n \tag{16a}$$

where, the kernel G_f and the external force F are given by

$$G_f(x_n,x_{nJ})=-\int_0^{x_n}\frac{\partial\chi}{\partial x_{nI}}(x_n,x_{nI})\hat{G}_{rn}(x_{nI},x_{nJ})dx_{nI} \tag{16b}$$

$$F(x_n)=2u_{e0n}\chi(x_n,0) \tag{16c}$$

for the functions χ and $\hat{G}_{rn}$ defined by

$$\begin{aligned}\chi(x_n,x_{nI})=&\left(-\sqrt{x_n+u_{e0n}{}^2}+\sqrt{x_{nI}+u_{e0n}{}^2}\right)\\ &\times\exp\left\{i\sqrt{2}\left(-\sqrt{x_n+u_{e0n}{}^2}+\sqrt{x_{nI}+u_{e0n}{}^2}\right)\Omega\right\}\end{aligned} \tag{16d}$$

$$\hat{G}_{rn}(x_{nI},x_{nJ})\equiv\int_0^{x_{nI}}\{G_r(x_{nI},x_{nJ})-G_\ell(x_{nI},x_{nJ})\}dx_{nI} \tag{16e}$$

where partial integration has been achieved for the calculation of the kernel G_f to remove the singularity of the kernels G_r and G_ℓ. The parameters governing the present phenomena are the aspect ratios h/L_r and h/L_ℓ, the non-dimensional frequency Ω, the initial velocity u_{e0n}, and the parameter Γ representing the effect of the air.

To see the oscillations of the water sheet observed in our experiments, the non-dimensional

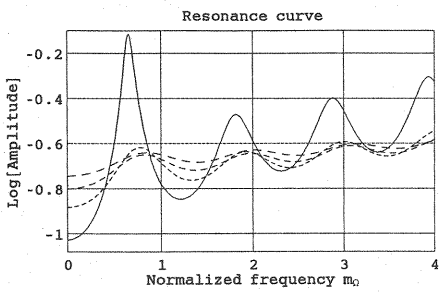

Fig. 8 Resonance curves
(Solid line is for h_e/h=0.005, and the larger the dash, the larger the value of h_e/h (0.01,0.015,0.02).)

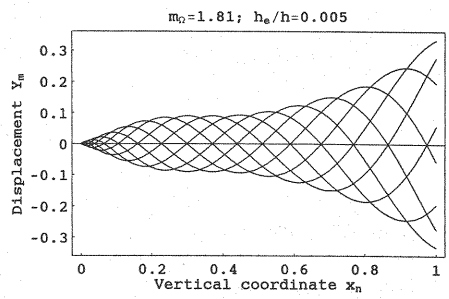

Fig. 9 Water sheet profiles
(Profiles at each $\Omega t_n = \pi/4$ time interval.)

parameters presented in the previous paragraph are estimated in terms of the water depth h_e above the weir crest. Using the rough estimates $u_{e0} \approx \sqrt{g_0 h_e}$, $2y_{e0} \approx h_e$, $L_r \approx T u_{e0}/2$ and $T \approx \sqrt{2h/g_0}$, where T is the time for a water particle to fall from the weir to the bottom, we have

$$q_n = \frac{2y_{e0}u_{e0}}{h\sqrt{g_0 h}} \approx \left(\frac{h_e}{h}\right)^{3/2} ; \quad u_{e0n} = \frac{u_{e0}}{\sqrt{2g_0 h}} \approx \left(\frac{h_e}{2h}\right)^{1/2}$$
$$\frac{L_r}{h} \approx \left(\frac{h_e}{2h}\right)^{1/2} ; \quad \frac{L_\ell}{h} \to -\infty \qquad (17)$$

As a result, the solution of Eq. 5a is completely determined from h_e/h and Ω.

The Schwartz criterion (Schwartz (1)) for resonance gives

$$\Omega/\sqrt{2} = \pi(m_\Omega + 1/4), \qquad m_\Omega = 0,\ 1,\ 2,\ \ldots \qquad (18)$$

Hence, in the following, m_Ω is used as the non-dimensional frequency instead of Ω. Figure 8 illustrates the resonance of the water sheet for various values of h_e/h by depicting the maximum amplitude of the water sheet as a function of m_Ω. The peaks are attained at non-integer points along the abscissa. The sheet profile for $h_e/h = 0.005$ and $m_\Omega = 2.2$ is plotted in Fig. 9 to see the effect of air on the water flow. The displacement of the sheet is amplified because of the Kelvin-Helmholtz instability, and the modulation of the amplitude occurs due to the waves propagating upstream. However, the maximum amplitude will not increase monotonically with respect to Γ since the added mass of air increases when Γ becomes larger, which suppresses the amplification.

The frequency of naturally occurring nappe oscillations might be selected among the resonance points shown in Fig. 8. However, the resonance frequencies in nature are not known and, of course, neither is the selection mechanism.

3.2 SHEAR WAVE INSTABILITY

In the present section, we investigated the shear wave instability of vertically falling water in an infinite region with no boundary, i.e., $|L_r|$, $|L_\ell|$ & $h \to \infty$ (see Fig. 7).

3.2.1 NONUNIFORM STEADY FLOW

First, the solution of the nonuniform steady flow is determined by applying the boundary layer approximation to the Navier-Stokes equations. The equations of this approximation for the water and air are

$$\frac{\partial u_w}{\partial x} + \frac{\partial v_w}{\partial y} = 0 \tag{19a}$$

$$\rho_w\left(u_w\frac{\partial u_w}{\partial x} + v_w\frac{\partial u_w}{\partial y}\right) - \mu_w\frac{\partial^2 u_w}{\partial y^2} - (\rho_w - \rho_a)g = 0 \tag{19b}$$

$$\frac{\partial u_a}{\partial x} + \frac{\partial v_a}{\partial y} = 0 \tag{20a}$$

$$\rho_a\left(u_a\frac{\partial u_a}{\partial x} + v_a\frac{\partial u_a}{\partial y}\right) - \mu_a\frac{\partial^2 u_a}{\partial y^2} = 0 \tag{20b}$$

where, u and v are respectively the flow velocities in the x and y directions, μ is the kinematic viscosity, and the subscripts "w" and "a" indicate the variables for the water and air, respectively. The boundary conditions at the interface between the water and air based on this approximation come from continuity of the flow velocities and tangential stress, and that of the free surface;

$$u_w = u_a \;;\quad v_w = v_a \;;\quad \mu_w\frac{\partial u_w}{\partial y} = \mu_a\frac{\partial u_a}{\partial y} \;;\quad u_w\frac{\partial \eta_\alpha}{\partial x} = v_w, \quad \text{at} \quad y = \eta_\alpha \tag{21}$$

Since the boundary layer thickness of the water flow, except in the near field close to the exit slit is large compared to the thickness of the water sheet, the variables for the water sheet are approximated by the truncated series as follows:

$$\begin{aligned} u_w(x,y) &\approx u_{w0}(x) + yu_{w1}(x) + y^2u_{w2}(x) \\ v_w(x,y) &\approx v_{w0}(x) + yv_{w1}(x) + y^2v_{w2}(x) + y^3v_{w3}(x) \end{aligned} \tag{22}$$

Now, to get the solution of the steady flow possessing symmetry with respect to the x-axis, i.e., $\eta_r = -\eta_\ell = Y_s$, $u_w(x,y) = u_w(x,-y)$ and $v_w(x,y) = -v_w(x,-y)$, the substitution of Eq. 22 into Eqs. 19a, 19b and 21 gives the following relations:

$$Y_s\left(u_{w0} + \frac{Y_s^2}{3}u_{w2}\right) = \frac{q}{2} \tag{23a}$$

$$\rho_w u_{w0}\frac{du_{w0}}{dx} - (\rho_w - \rho_a)g - 2\mu_w u_{w2} = 0 \tag{23b}$$

$$u_a\big|_{y=Y_s} = u_{w0} + Y_s^2u_{w2} \;;\quad v_a\big|_{y=Y_s} = \frac{dY_s}{dx}\left(u_{w0} + Y_s^2u_{w2}\right) \tag{23c}$$

$$\left.\frac{\partial u_a}{\partial y}\right|_{y=Y_s} = \frac{\mu_w}{2\mu_a}Y_s u_{w2} \tag{23d}$$

where, q is the discharge of unit width from the slit. Since the system of Eqs. 20a and 20b is a parabolic type, two boundary conditions at $y = Y_s$ and one boundary condition at $x = 0$ are necessary and sufficient to determine the solution. Assuming that the solution of the air-flow equations given

by Eqs. 20a and 20b is obtained under the boundary conditions given by Eq. 23c and $u_a|_{x=0} = 0$, the derivative $\partial u_a / \partial y|_{y=Y_s}$ is a function of Y_s, u_{w0} and u_{w2}. Therefore, Eq. 23d is one of the governing equations for the three unknowns Y_s, u_{w0} and u_{w2}. As a result, Eqs. 23a, 23b and 23d completely determine these three unknown variables.

Equations 23a, 23b, 23c and 23d can be simplified by estimating the magnitude of u_{w2} from Eq. 23d. Assuming that $q \sim u_{w0} Y_s$, i.e., $u_{w0} >> Y_s^2 u_{w2}$, in Eq. 23a, Eq. 23d leads to the following estimate:

$$\mu_w u_{w2} \sim \frac{\mu_a}{\mu_w} \frac{1}{R_{ew}} \frac{x}{\delta_a} \frac{\rho_w u_{w0}^2}{x} \quad ; \quad \delta_a \sim \sqrt{\frac{\mu_a x}{\rho_a u_{w0}}} \quad ; \quad R_{ew} \equiv \frac{\rho_w q}{\mu_w} \tag{24}$$

where, δ_a is the boundary layer thickness of the air. By applying the estimate given by Eq. 24 to Eq. 23a, the validity of the assumption $q \sim u_{w0} Y_s$ is justified as indicated in the following estimate:

$$\frac{Y_s^2 u_{w2}}{u_{w0}} \sim \left(\frac{\rho_a}{\rho_w}\right)^{1/2} \left(\frac{\mu_a}{\mu_w}\right)^{1/2} R_{ew}^{1/2} \left(\frac{Y_s}{x}\right)^{1/2} << 1 \tag{25}$$

noting that, $R_{ew} = O(10^3)$ in our experiment. Therefore, Eqs. 23a, 23b, 23c and 23d can be reduced to the following equations:

$$Y_s u_{w0} = \frac{q}{2} \tag{26a}$$

$$\rho_w u_{w0} \frac{du_{w0}}{dx} - (\rho_w - \rho_a) g = 0 \tag{26b}$$

$$u_a|_{y=Y_s} = u_{w0} \quad ; \quad v_a|_{y=Y_s} = \frac{dY_s}{dx} u_{w0} \tag{26c}$$

$$\left.\frac{\partial u_a}{\partial y}\right|_{y=Y_s} = \frac{\mu_w}{2\mu_a} Y_s u_{w2} \tag{26d}$$

Substitution of the solutions of Eqs. 26a and 26b into Eq. 26c gives the boundary conditions for Eqs. 20a and 20b.

A change of the coordinates from (x, y) to $(x, y - Y_s)$ and the introduction of the stream function ψ_a for u_a and v_a reduce Eqs. 20a and 20b to

$$\frac{\partial \psi_a}{\partial Y} \frac{\partial^2 \psi_a}{\partial x \partial Y} - \frac{\partial \psi_a}{\partial x} \frac{\partial^2 \psi_a}{\partial Y^2} = \frac{\mu_a}{\rho_a} \frac{\partial^3 \psi_a}{\partial Y^3} \quad ; \quad Y \equiv y - Y_s$$

$$u_a = \frac{\partial \psi_a}{\partial y} \quad ; \quad v_a = -\frac{\partial \psi_a}{\partial x} \tag{27}$$

Here, the boundary conditions given by Eq. 26c for Eq. 27 become

$$\left.\frac{\partial \psi_a}{\partial Y}\right|_{Y=0} = \sqrt{2 g_0 x + u_{e0}^2} \quad ; \quad \psi_a|_{Y=0} = const. \tag{28}$$

Note that the stream function representation of Eqs. 20a and 20b is invariant under translation of the variable y. If we consider the region of the flow field in which $2g_0x >> u_{e0}^2$ is satisfied, which is valid in the flow field except in the narrow field close to the weir crest because $u_{e0} \sim \sqrt{g_0 h_e}$ for the weir flow, the solution of Eqs. 27 and 28 is represented by the Falkner-Skan similarity solution (Shlichting (17)):

$$\psi_a \approx u_{w0}\sqrt{\frac{4}{3}\frac{\mu_a x}{\rho_a u_{w0}}}f(\xi) \;;\quad \xi = Y\sqrt{\frac{3}{4}\frac{\rho_a u_{w0}}{\mu_a x}} \;;\quad u_{w0} \approx \sqrt{2g_0 x}$$

$$\frac{d^3 f}{d\xi^3} + f\frac{d^2 f}{d\xi^2} - \frac{2}{3}\left(\frac{df}{d\xi}\right)^2 = 0 \;;\quad f|_{\xi=0} = 0 \;;\quad \left.\frac{df}{d\xi}\right|_{\xi=0} = 1 \;;\quad \left.\frac{df}{d\xi}\right|_{\xi\to\infty} = 0 \tag{29}$$

Therefore, the Falkner-Skan similarity solution (Shlichting (17)) and the parabolic velocity profile are respectively used for the steady flow in the air and in the water. It should be noted that this was checked numerically, and that the air-flow is well-approximated by the above solution (Kyotoh and Kase (11)).

3.2.2 LINEAR STABILITY ANALYSIS OF LOCALLY UNIFORM FLOW

Although the flow obtained in 3.2.1 is in reality spatially nonuniform, we consider regions in the flow small enough, such that, the flow may be considered locally uniform and parallel. As a result, a temporal linear stability analysis of the Navier-Stokes equations can be applied to this two-phase flow. In order to calculate the eigen-values for the temporal growth of disturbances, the Riccati equation method (Davy (18)) was applied in this study.

Figure 10 shows the wavelength and frequency of the unstable sinuous mode of the flow corresponding to the velocity distributions of the sheet of falling water at x = 100 cm and 150 cm. Here, surface tension and the viscosities of air and water were incorporated in the calculation. The mode depicted in Fig. 10 is not the surface wave mode, for which the frequency is much higher and the wavelength is shorter, but the shear wave mode. As the height of the water sheet increases from 100 cm to 150 cm, the frequency of the unstable mode decreases and its wavelength becomes longer. Looking at the spectra of Fig. 2, the peak value at x = 120 cm is around 10 Hz or 15 Hz for h_e = 2.12 and 3.47 cm, which are approximately the same as the critical frequencies predicted by this analysis.

Though the theoretical predictions seem to be fairly accurate in representing the situation, many

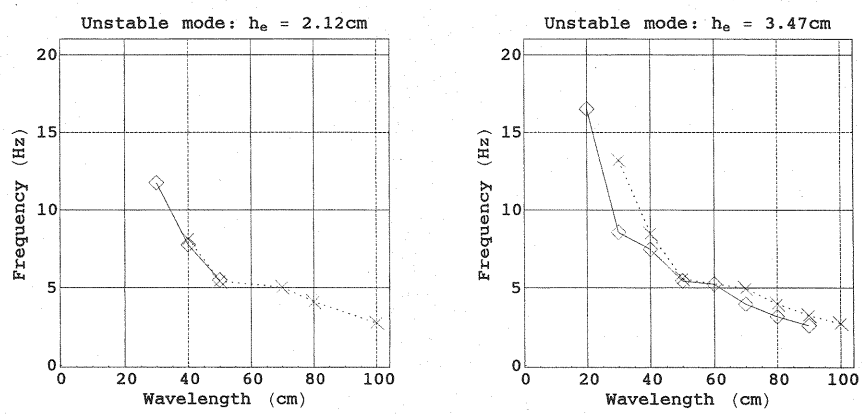

Fig. 10 Wavelength and frequency of the unstable sinuous mode
(Diamond and cross symbols show the values at x = 100 cm and 150 cm, respectively. The water depth above the weir-crest is denoted by h_e.)

unstable modes exist in the upper region of the sheet as well, according to our locally uniform-flow-approximation, and these have higher frequencies. Also, the frequency around 30 Hz leading to the sheet breakup is not explained in the present study. In order to understand the breakup, the nonlinear stability of nonuniform flow needs to be examined.

4. CONCLUSIONS

The stability of a sheet of falling water from a weir was studied both experimentally and theoretically. The free-fall experiments described in section 2.2.1 indicate that a supercritical transition of the sheet oscillations occurs downstream and the amplitude of oscillation increases exponentially. The forced-vibration experiments described in section 2.2.2 siggest that the frequency response of the sheet, as measured by the transverse oscillations of the sheet, varies with position along the sheet and therefore with the thickness of the sheet, with the sheet resonating at higher frequencies in the thinner section of the sheet, i.e., at greater distances from the weir crest. This suggests that the instability leading to the sheet breakup might be primarily caused by events occurring near the breakup region even though some strong transitory oscillations are seen further upstream. The experiments with the back-wall in section 2.2.3 indicate that, the air confined between the walls and the water sheet causes a modulation of the sheet amplitude.

Taking into account the observations in the back-wall experiments, a model describing the motion of the sheet in the longitudinal and normal directions for the back-wall case was developed assuming that the flow was irrotational. This model explains the amplification of the sheet oscillations and the modulation of the amplitude of oscillation caused by the propagation of pressure fluctuations under the influence of the confined air. In addition, incipient oscillations of the sheet observed in the free-fall experiments, which could be shear waves appearing on the sheet, were characterized in section 3.2 by using a uniform-flow model subjected to a linear stability analysis of the corresponding Navier–Stokes equations. The linear stability analysis of the uniform-flow model reveals a critical frequency of local oscillation of the sheet beyond which an oscillation induced by shear waves will grow. As for the region around 120 cm below the weir crest, this critical frequency of local oscillation agrees quite well with the measured frequency of local oscillation of the actual non-uniform sheet, thereby providing a mean for predicting the frequency at the region of onset of oscillations of the sheet of water, i.e., the incipient oscillations. Below this region, the dominant frequency of the measured oscillations increases to two or three times the frequency of the incipient oscillations, so it is not yet possible to predict the region of onset of breakup. However, this qualitative agreement provides evidence that by extending our model by incorporating global effects, including perhaps nonlinear dynamics, we may, in the near future, be able to adequately characterize theoretically the growth of oscillations and the region of onset of breakup of the sheet of water.

ACKNOWLEDGEMENTS

We are indebted to Professor H. Nishimura for his continuous discussions of the present topic. The first author is grateful to Professor K. Matsuuchi for his helpful comments on the instability theory of liquid jets. Also, we appreciate the members of our staff, Messrs T. Nakajima, M. Iidaka, A. Kojima, K. Yamada and H. Terada, for their support in setting up the falling-water facility. Finally, the first author appreciates Mr. Thomas Copeland for checking the manuscript. This work was supported in part by the Grants in Aid for Scientific Research (C) of JSPS.

REFERENCES

1. Shwartz, H.I. : Projected nappes subjected to harmonic pressures, Proc. Inst. Civil Engineers, Vol.28, pp.313-326, 1964.
2. Binnie, A.M. : The stability of a falling sheet of water, Proc. R. Soc. London, A.326, pp.149-163, 1972.

3. Honma, M. and K. Ogiwara : Theoretical analysis of flap gate oscillation, JSCE, No.238, pp.43-53, 1975 (in Japanese).
4. Casperson, L.W. : Fluttering fountains, J. Sound and Vibration, Vol.162(2), pp.251-262, 1993.
5. Weinstein, S.J., A. Clarke, A.G. Moon and E.A. Simister : Time-dependent equations governing the shape of a two-dimensional liquid curtain, Part 1 : Theory, Phys. Fluids, Vol.9(12), pp.3625-3636, 1997.
6. Luca, de L. : Experimental investigation of the global instability of plane sheet flows, J. Fluid Mech., Vol.399, pp.355-376, 1999.
7. Laheras, J.C. and E.J. Hopfinger : Liquid jet instability and atomization in a coaxial gas stream, Ann. Rev. Fluid Mech., Vol.32, pp.275-308, 2000.
8. Taylor, G.I. : The dynamics of thin sheet of fluid, II. Waves on fluid sheets, Proc. R. Soc. London, Vol.A253, pp.296-312, 1959a.
9. Taylor, G.I. : The dynamics of thin sheet of fluid, III. Disintegration of fluid sheets, Proc. R. Soc. London, Vol.A253, pp.313-321, 1959b.
10. Mansour, A. and N. Chigier: Dynamic behavior of liquid sheets, Phys. Fluids, Vol.A3 (12), pp.2971-2980, 1991.
11. Kyotoh, H. and N. Kase : A study on the oscillations of a falling water sheet, Rep. RIAM Sym., No.12 ME-S2, pp.46-55, 2000 (in Japanese).
12. Aizawa, M., Shinohara, O. : An experimental study on the texture of falling water of free falling and slope falling types, JSCE, 593/II-43, pp.105-115, 1998 (in Japanese).
13. Hagerty, W.W. and Shea, J.F. : A Study of the Stability of Plane Fluid Sheets, J. Applied Mech., Vol.22, pp.509-515, 1955.
14. Lin, S.P. : Stability of a viscous liquid curtain, J. Fluid Mech., Vol.104, pp.111-118, 1981.
15. Luca, de L. and M. Costa : Instability of a spatially developing liquid sheet, J. Fluid Mech., Vol.331, pp.127-144, 1997.
16. Finnicum, D.S., S.J. Weinstein and K.J. Ruschak : The effect of applied pressure on the shape of a two-dimensional liquid curtain falling under the influence of gravity, J. Fluid Mech., Vol.255, pp.647-665, 1993.
17. Schlichting, H. : Boundary Layer Theory, McGraw-Hill, 647p., 1962.
18. Davy, A. : On the numerical solution of difficult eigen value problems, J. Comput. Phys., Vol.24, pp.331-338, 1977.

APPENDIX — NOTATION

The following symbols are used in this paper:

A_{Ym} = complex amplitude of the displacement of the water sheet;
f = dimensionless stream function defined by Eq. 30;
g = gravity acceleration;
g_0 = $(1-\rho_a/\rho_w)g$;
G_α = Green's function defined by Eq. 7;
G_f = Green's function defined by Eq. 16b;
G_r, G_ℓ = Green's functions G_α for $\alpha = r$ and ℓ;
$\hat{G}_{rn}$ = Green's function defined by Eq. 16e;
h_e = water depth above the weir;
h = height of the back-wall from the weir crest;
m_Ω = dimensionless frequency defined by Eq. 18;
L_α = position of the side walls;
P_w = pressure of the water;
$P_{S\alpha}$ = air pressure at the interface;
$P_{S\alpha 0}, P_{S\alpha 1}$ = coefficients of the terms in the series of $P_{S\alpha}$ with respect to δ;
q = discharge of flow from the unit width of the exit slit;
q_n = dimensionless form of q;
Q = discharge from the weir;
R_{ew} = Reynolds number of the water at the exit slit defined by Eq. 24;
S = surface tension coefficient;
t = time;
$\bar{t}$ = integral variable of t;
t_n = dimensionless form of t;
T = time of free fall;
u_a = air velocity of the viscous flow in the x-direction;
u_{e0} = flow velocity at the exit slit;
u_w = water velocity of the viscous flow in the x-direction;
u_{w0}, u_{w1}, u_{w2} = coefficients of the terms in the series of u_w with respect to y;
U_w = water velocity of the potential flow in the x-direction;
v_a = water velocity of the viscous flow in the y-direction;
v_w = air velocity of the viscous flow in the y-direction;
v_{w0}, v_{w1}, v_{w2} = coefficients of the terms in the series of v_w with respect to y;
V_w = water velocity of the potential flow in the y-direction defined by Eq. 5c;
W_b = Weber number defined by Eq. 10;
x = distance from the weir crest downstream;
$\bar{x}$ = integral variable of x;
x_n = dimensionless form of x;
x_{nI}, x_{nJ} = integral variable of x_n;
x_{nS} = position of the singular point defined by Eq. 14;

y = horizontal distance from the vertical plane;
y_{e0} = half thickness of the water sheet at the exit slit;
Y_m = lateral displacement of the water sheet;
Y_s = half thickness of the water sheet;
α = coefficient, i.e., either "r" for the right or "ℓ" for the left hand side of the water sheet;
$\gamma = \rho_a / \rho_w$ = density ratio;
Γ = parameter representing the effect of the air defined by Eq. 16a;
$\delta = \varepsilon^2$ = small parameter representing the non-uniformity of the flow;
δ_a = boundary layer thickness of the air;
Δ = two-dimensional Laplace operator;
ε = ratio between the length scales of the flow in the x and y directions;
η_α = displacement of the water sheet;
$\eta_{\alpha 0}, \eta_{\alpha 1}$ = coefficients of the terms in the series of η_α with respect to δ;
κ_α = curvature of the interface;
μ_a = viscosity of air;
μ_w = viscosity of water;
ξ = similarity variable defined by Eq. 30;
ρ_w = water density;
ρ_a = air density;
τ = intermediate parameter ranging in value from 0 to t;
$\phi_{S\alpha}$ = velocity potential at the interface;
ϕ_w = velocity potential of the water sheet;
ϕ_{w0}, ϕ_{w1} = coefficients of the terms in the series of ϕ_w with respect to δ;
χ = function defined by Eq. 16d;
ψ_a = stream function of the air defined by Eq. 28; and
Ω = dimensionless angular frequency, respectively.

(Received July 13, 2001 ; revised September 16, 2001)